Accepted Manuscript

Defects guided wrinkling in graphene on copper substrate

Zhenqian Pang, Bing Deng, Zhongfan Liu, Hailin Peng, Yujie Wei

PII:	S0008-6223(18)31090-X
DOI:	10.1016/j.carbon.2018.11.059
Reference:	CARBON 13676
To appear in:	*Carbon*
Received Date:	17 August 2018
Accepted Date:	20 November 2018

Please cite this article as: Zhenqian Pang, Bing Deng, Zhongfan Liu, Hailin Peng, Yujie Wei, Defects guided wrinkling in graphene on copper substrate, *Carbon* (2018), doi: 10.1016/j.carbon.2018.11.059

Defects guided wrinkling in graphene on copper substrate

Zhenqian Pang[1,4], *Bing Deng*[2], *Zhongfan Liu*[2,3*],*Hailin Peng*[2,3*], *Yujie Wei*[1,4*]

[1]LNM, Institute of Mechanics, Chinese Academy of Sciences, Beijing, 100190, People's Republic of China

[2] Center for Nanochemistry (CNC), Beijing National Laboratory for Molecular Sciences (BNLMS), College of Chemistry and Molecular Engineering, Peking University, Beijing 100871, China.

[3] Beijing Graphene Institute (BGI), Beijing 100094, China

[4] School of Engineering Sciences, University of Chinese Academy of Sciences, Beijing 100049, China

* Correspondence should be addressed to: yujie_wei@lnm.imech.ac.cn (Y.W.) or hlpeng@pku.edu.cn (H.P.), or zfliu@pku.edu.cn (Z.L.)

Abstract

Pristine graphene depositing on metallic substrates often wrinkles when the film-substrate system undergoes a temperature drop from the chemical vapor deposition (CVD) chamber to ambient environment. The pattern of wrinkles is governed by the crystallographic planes of the substrates and the defects in the film. In this paper, we report how commonly seen Stone-Wales defects and grain boundaries (GBs) influence the morphology of graphene on different planes of single crystalline copper substrate. Stone-Wales defects weaken the bending stiffness in graphene, and result in wrinkling along the defect direction. In the presence of GBs, primary wrinkles are always parallel to the GB direction, and there are also secondary wrinkles perpendicular to the GB. In combination with planes of the substrate and the orientation of defects, we demonstrate that we may manipulate wrinkling patterns for possible engineering applications.

Keywords: Wrinkling, Graphene, Grain boundary, Stone-Wales defects, Binding energy

1. Introduction

Chemical vapor deposition (CVD) as traditional growth method of graphene has been extensively applied on various metal substrates [1-3]. As we cool down the system at the CVD temperature to room temperature, the difference between the thermal expansion of graphene and that of the metallic substrate induces compressive stress in graphene, and sequentially forces graphene to buckle to the unconstrained side [4, 5]. Such morphology change may cause mechanical strength and thermal conductivity reduction [6-8], as well as electrical properties: wrinkles affect the lateral current transport when graphene transfer on an insulating substrate; while the influence to vertical current transport is observed on metallic and semiconductor substrates [7, 9, 10]. It has been observed that graphene films on different kinds of metal substrate exhibit different morphology [1, 3, 11], and even for the same type of substrates, different crystallographic planes give rise to different morphology characteristics [12]. Furthermore, the surface structure of substrates dominate the initial nucleation and growth dynamics of graphene [13], and hence the quality of graphene films [14]. Since large-area monolayer graphene growth by CVD involves the decomposition of carbon source gases, such as CH_4 and C_2H_4 [13], and then the recombination of these carbon atoms, the presence of defects in large-area graphene films is inevitable: edges, grain boundaries (GBs) and Stone-Wales (SW) defect [1, 15-18] were commonly observed in CVD graphene. While edge effect has been intensively investigated [19-21], how an array of defects in graphene influences the morphology of CVD graphene remains unknown.

The formation of wrinkles plays an important role in the preparation of graphene and it mainly occurs in the process of growth and transfer. Many intrinsic and external factors may alter wrinkling. For example, the surface structure of the substrates affects the growth dynamics graphene and hence [13] its wrinkling. Previous researches showed us that adoption of corrugated substrates can avoid wrinkling formation effectively during the transfer process [22]. The interaction between the graphene and the substrate will of course influence wrinkling as well. Strong bonding

between graphene and the substrate can effectively suppress thermally assisted wrinkles [23]. For the most common CVD growth involving graphene and copper substrate, there is a strong interaction between the two materials [12]. However, in the presence of GBs and SW defects, they may enhance or weaken the interaction, resulting in rich wrinkling patterns. Meanwhile, the defects alter the bending stiffness [24, 25] of graphene and hence render the growth of wrinkles easier.

In this paper, we focus on the intrinsic factor governing wrinkling in graphene and consider the correlation between defects and wrinkling in graphene films grown on copper substrate. We explored how the density and distribution of defects like Stone-Wales arrays and GBs [26] impact the wrinkling of graphene on different crystallographic planes of copper substrate. We first introduce the computational methods in Section 2. The simulation results are then presented in Sections 3 and 4, with the former for Stone-Wales arrays and the latter for grain boundaries. Results from experimental observation are then supplied in Section 5, where the statistical nature of wrinkling is explored, and the morphology of wrinkles matches reasonably well with simulation results. We conclude in Section 6 with final remarks.

2. Computational Methods

At the depositing temperature, a graphene sheet is initially flat on the copper substrate. The mismatch strain ε in the graphene layer as temperature decreases, is estimated as $\varepsilon = (\alpha_{cu} - \alpha_{g})\Delta T$, here α_{cu} and α_{g} represent respectively the coefficient of thermal expansion of copper substrate and graphene, the value of each is $(-8.0 \pm 0.7) \times 10^{-6}$ K^{-1} [5] and $(16.5 \pm 0.2) \times 10^{-6}$ K^{-1} [27], and ΔT is temperature gradient.

Large-scale molecular dynamics (MD) simulations using the massively parallel simulator (LAMMPS) [28] was performed to understand the interaction between graphene films and copper substrates and the resultant wrinkling in CVD growth. The adaptive intermolecular reactive empirical bong order (AIREBO) [29] potential was used to describe the interaction among carbon atoms in graphene. The Cu-Cu interaction in copper substrate were represented by embedded atom method (EAM)

potential [30], which can accurately describe the structural and mechanical properties of Cu and is broadly accepted in such similar calculation. The interaction between C-Cu atoms is described by the Lennard-Jones (L-J) 6-12 potential, $V(r) = 4\phi(\sigma^{12}/r^{12} - \sigma^{6}/r^{6})$. Here ϕ and σ respectively characterize the depth of the potential well and the equilibrium position of the pair potential, and r is the distance between atomic pairs. In our MD simulations, we adopted ϕ=0.0168 eV and σ=2.2 Å [31, 32]; the corresponding potential captures well with the graphene-Cu interaction [33]. Time step was set as 0.5fs and a Nose-Hoover thermostat was used to maintain the NVT ensemble. The size of a defective graphene sheet composed of Stone-Wales arrays was about 70 nm by 70 nm. The size of the defective sample with embedded grain boundaries was about 100 nm by 60 nm. Periodical boundary condition was employed to all these samples. We set the initial CVD temperature of the graphene-Cu system at 1300 K and then cool the system to room temperature (300 K). Such a process introduces a compressive strain ε about 2.5% due to thermal mismatch.

The first principle calculation can be used to obtain an accurate bending stiffness of defective graphenes. The Vienna Ab initio Simulation Package (VASP) code [34, 35] for density functional theory (DFT) calculations was employed. The projector augmented wave (PAW) pseudopotentials [36, 37] and the generalized gradient approximation (GGA) of the Perdew-Burke-Ernzerhof (PBE) functional [38, 39] were used. A kinetic-energy cut-off of plane-wave basis was set as 520 eV. Following the same procedure to obtain the bending stiffness in reference [40], we construct defective carbon nanotubes with the chirality of (6, 6) and (8, 0) [41, 42]. The Monkhorst-Pack [43] k-point mesh of $2 \times 2 \times 8$ were used for those calculations. To eliminate the periodic images of system in radial direction, the size of box was set to 20Å so that the vacuum space between tubes was far greater than the cut-off distance. Periodic boundary condition was applied to axial direction. We chose two types of defective interface in graphene, the Stone-Wales arrays [17] and grain boundaries [18] for our simulations, and both were observed in the CVD growth of graphene sheets.

3. Wrinkling in Graphene with Stone-Wales Arrays

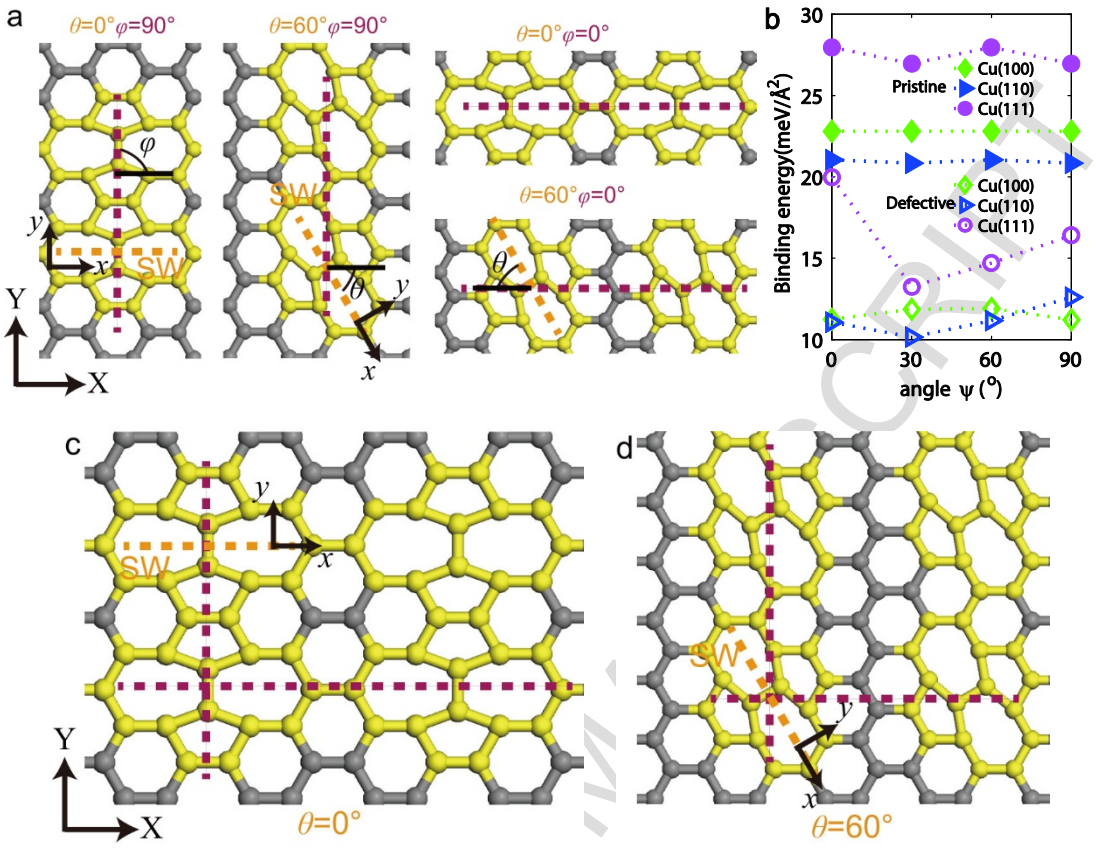

Fig.1 The distribution of Stone-Wales arrays (SWA) and the binding energy of graphene-Cu substrate in the presence of SWAs. (a) The arrangement of SW defects in graphene. We define a global coordinate X-Y, which is attached to graphene, and the X-axial is along the armchair direction and the Y-axis is along the zigzag direction of the graphene. A local *x*-*y* coordinate is used to characterize a single SW defect, with x-axis being the middle line of the heptagon rings. Hence the direction of a SWA is defined by two angles: the counter clock-wise rotation θ of *x*-*y* w.r.t. X-Y coordinate and the orientation Φ of the SWA w.r.t. the *x*-*y* coordinate which measures from the *x*-axis. We show several SWAs with different combination of (θ, Φ). (b) The dependence of binding energy of graphene with high density SWAs (θ = 0°) on Cu substrate plane and the relative orientation of graphene and substrate crystallographic plane, with ψ the angle between the X-axis (in graphene) and the [0 1 0], [0 0 1] and [1 1 -2] directions in Cu (100), Cu (110) and Cu (111) planes, respectively. The typical arrangement of graphene with high density SWAs: (c) θ = 0° and (d) θ = 60°.

The relative orientations among the substrate, the graphene, and the SWA need to be specified in advance, in order to explore the influence of SW defects on morphology of graphene directly. We defined the global coordinate (X-Y) along armchair-zigzag direction in pristine graphene and a local coordinate (*x*-*y*) based on a single SW defect. Hence the relative rotation between (X-Y) and (*x*-*y*) characterizes the direction of a single SW defect; and (x-y) is used to characterize the orientation between a single SW defect and the SW array: the first rotation is defined as θ and the second angle is defined as φ, as detailed in Fig.1 (a). The orientation of a graphene layer on a Cu substrate with respect to the crystalline orientation was defined by a particular orientation in the Cu crystallographic plane with respect to the armchair direction (X-axis) of the graphene.

The presence of defect arrays would change the interaction between the graphene and the substrate. In Fig. 1b, we present the binding energy between a free graphene with high density SWAs ($\theta = 0°$) on different Cu substrate planes. It is noted that there is another degree of freedom which may alter the binding energy, the relative orientation of graphene and substrate crystallographic plane. We define ψ the angle between X-axis (in graphene) and a particular direction in Cu substrate. For Cu (100), Cu (110) and Cu (111) substrates, we choose [0 1 0], [0 0 1] and [1 1 -2] in the three respective crystallographic planes. It is seen from Fig. 1b the energy of SW defects adhering to Cu(100), Cu(110) and Cu(111) is much lower than that of pristine graphene adhering on copper substrates [12, 31].

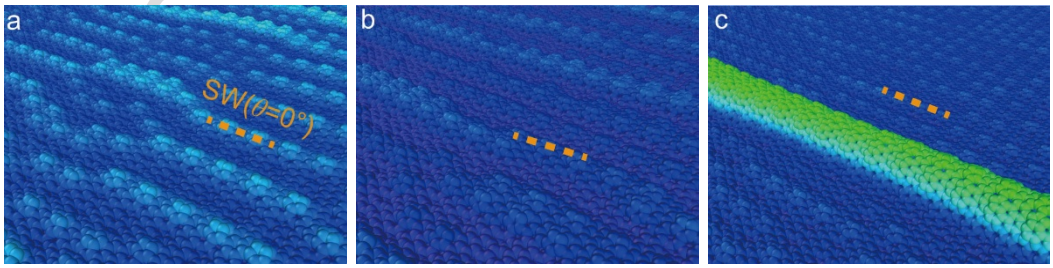

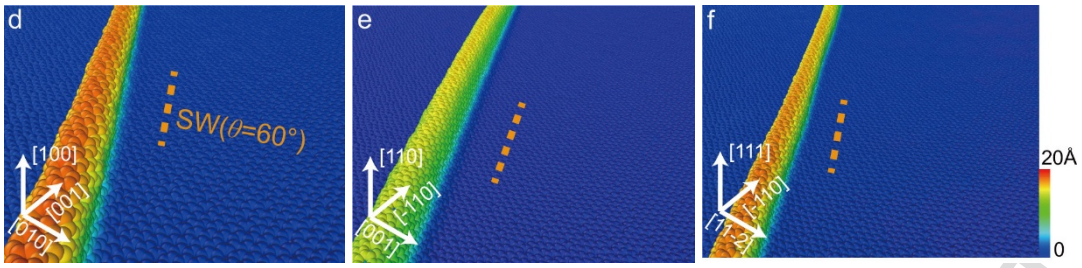

Fig. 2 The morphology of graphene in the presence of high density of Stone-Wales arrays (SWA). (a) to (f) The morphology of different SWAs residing in Cu(100), Cu(110) and Cu(111) substrates: (a) to (c) graphene with SWAs of $\theta = 0°$ and (d) to (f) graphene with SWAs of $\theta = 60°$. At the high density limit, ϕ does not affect the final morphology due to lattice symmetry.

We first simulated the graphene with the maximum Stone-Wales arrays (SWAs) along both X and Y directions ($\theta = 0°$ and $60°$, $\phi = 0°$ and $90°$) (Fig.1 (a)), whose defect density is about 33.3% and 50%. For these cases, the orientation of two adjacent defects along X-direction and Y-direction are both maximum and φ does not affect the morphology at all, as seen in Figs. 1(c) and (d). Hence we will only supply θ for structures shown in Figs. 1(c) and (d). In our previous work [12], wrinkle is seen in graphene grown on Cu(100) and Cu(110) substrate, while the wrinkle-free graphene appeared on Cu(111). In the presence of SWAs ($\theta = 0°$), wrinkle-free graphene on both Cu(100) and Cu(110) is possible, as seen in Figs. 2(a) and (b). In contrast, a wrinkle appears along the defect array when the graphene is on Cu (111), as shown in Fig. 2(c). It is noted that even for the wrinkle-free graphene (Figs. 2(a) and (b)), SW defects form small tents to release the compressive stress in the film and hence lower its strain energy. When the SWAs are of $\theta = 60°$, wrinkling occurs in all three planes of the Cu substrate, as shown in Figs. 2(d) to (f). The wrinkles are parallel to the SW direction.

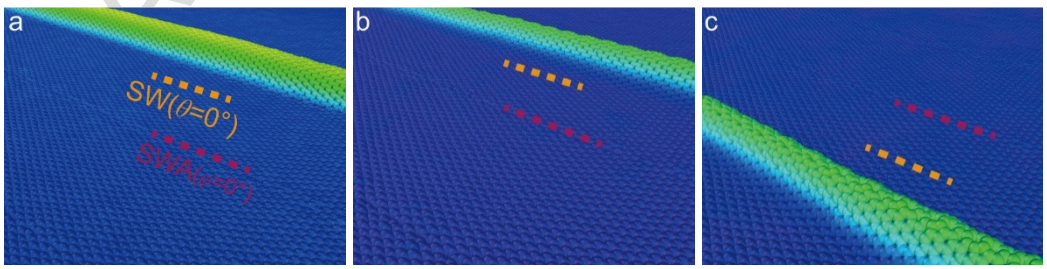

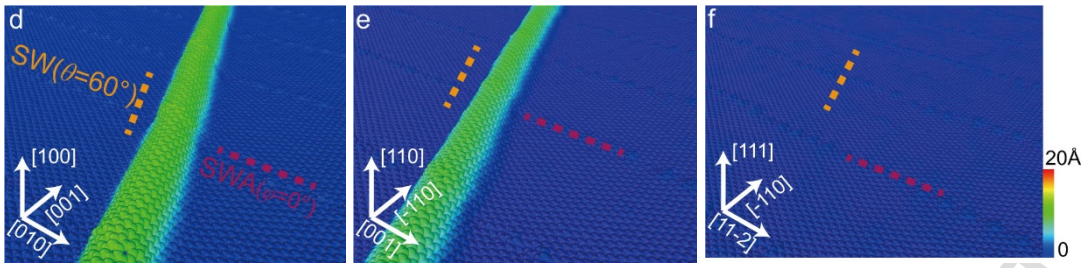

Fig.3 The morphology of graphene in the presence of low density of SWAs. (a) to (f) The morphology of different SWAs residing in Cu (100), Cu (110) and Cu (111) substrates: (a) to (c) graphene with SWA as $\theta = 0^{o}$, $\phi = 0^{o}$ and (d) to (f) graphene with SWA of $\theta = 60^{o}$, $\phi = 0^{o}$.

As we pointed out at the beginning, both the orientation of SWs and the direction of the SWA affect wrinkling. To analyze how the direction of SWAs influences the morphology of graphene, we simulated the graphene films with low density of defects. By counting the fraction of non-hexagonal rings in a sample, we first used a sample with 3.33% of defects for $\theta = 60°$, $\phi = 0°$ and 5% for $\theta = 0°$, $\phi = 0°$. We first show the results from the sample with $\theta = 0°$, $\phi = 0°$. Here wrinkles are parallel to the array direction, as evidently seen in Figs. 3(a) to (c) for Cu(100), Cu(110) and Cu (111) substrates, respectively. When the angle between the orientation of SW and X-direction is $\theta = 60°$, $\phi = 0°$, competing factors including the SW direction, SWA direction, and the binding energy of different Cu substrate planes influence wrinkling. Wrinkles extend along the SW array on the Cu(100) and Cu(110) planes, see Figs. 3(d) and (e) respectively. In contrast, wrinkling is nearly suppressed when the graphene resides on Cu(111) (see Fig. 3(f)), similar to what we see for pristine graphene on Cu(111).

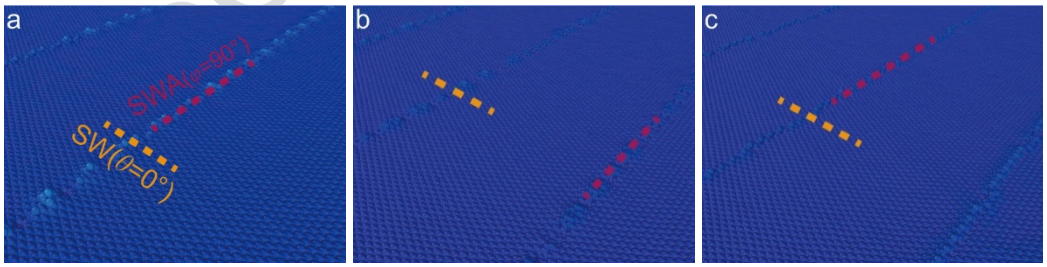

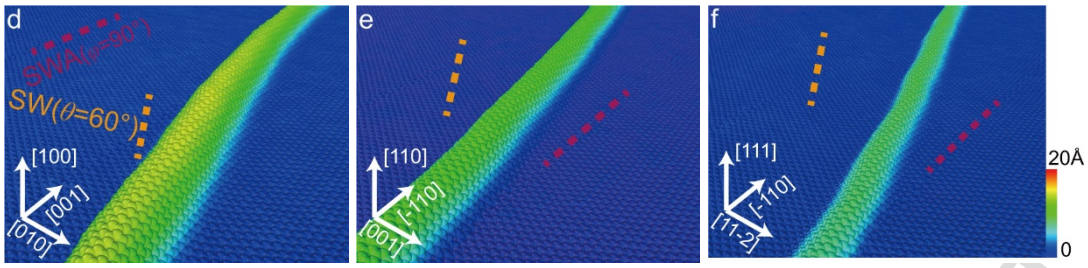

Fig.4 The morphology of graphene in the presence of low density of SWAs. (a) to (f) The morphology of different SWAs residing in Cu (100), Cu (110) and Cu (111) substrates: (a) to (c) graphene with SWA as $\theta = 0°$, $\phi = 90°$ and (d) to (f) graphene with SWA as $\theta = 60°$, $\phi = 90°$.

When the SWA is arranged with $\theta = 0°, \varphi = 90°$ and $\theta = 60°, \varphi = 90°$, the morphology of graphene is significantly different from pristine graphene. Figures 4(a) to (c) show the atoms arrangements with the tilt angle of SW defects as $\theta = 0°$, $\phi = 90°$, where the orientation of individual SWs is perpendicular to the array direction, even at very low defect density. When the orientation of SWs and SWA are not perpendicular, $\theta = 60°$, $\phi = 90°$, the competition leads to the formation of wrinkles between the orientation of SWs and SWAs, as shown in Figs. 4(d)~(f).

As the orientation of both SW and also SWAs influence local bending stiffness of graphene, we calculate the bending stiffness of pristine and defective graphene based on DFT calculations. Similar to pristine graphene [40], we roll a single-layer defective graphene sheets to nanotubes (Figs. 5(a) (b)) of different radius and along different chirality. Their bending stiffness is obtained using the equation [40, 44]:

$$B = 2(E_{tube} - E_G)r^2/S_0$$

where B is the bending stiffness of graphene, E_{tube} and E_G represent the energy of tube and graphene, S_0 is the area of planar graphene, r is the radius of a tube. Figure 5(c) shows the bending stiffness of pristine and defective graphene with different chirality. While the bending stiffness of pristine graphene is positive [40, 44], that of defective graphene is negative. It implies the defective graphene prefers to bend, and the energy along different chirality exhibits slight difference: the value with the x-axis of a SW

parallel to the tube axis is about -0.98 eV, and is lower than that when the *y*-axis of the SW is along the tube axis (-0.71 eV). The negative bending stiffness of tubes with SWs demonstrates why defective graphene prefers to form wrinkles along the SWAs.

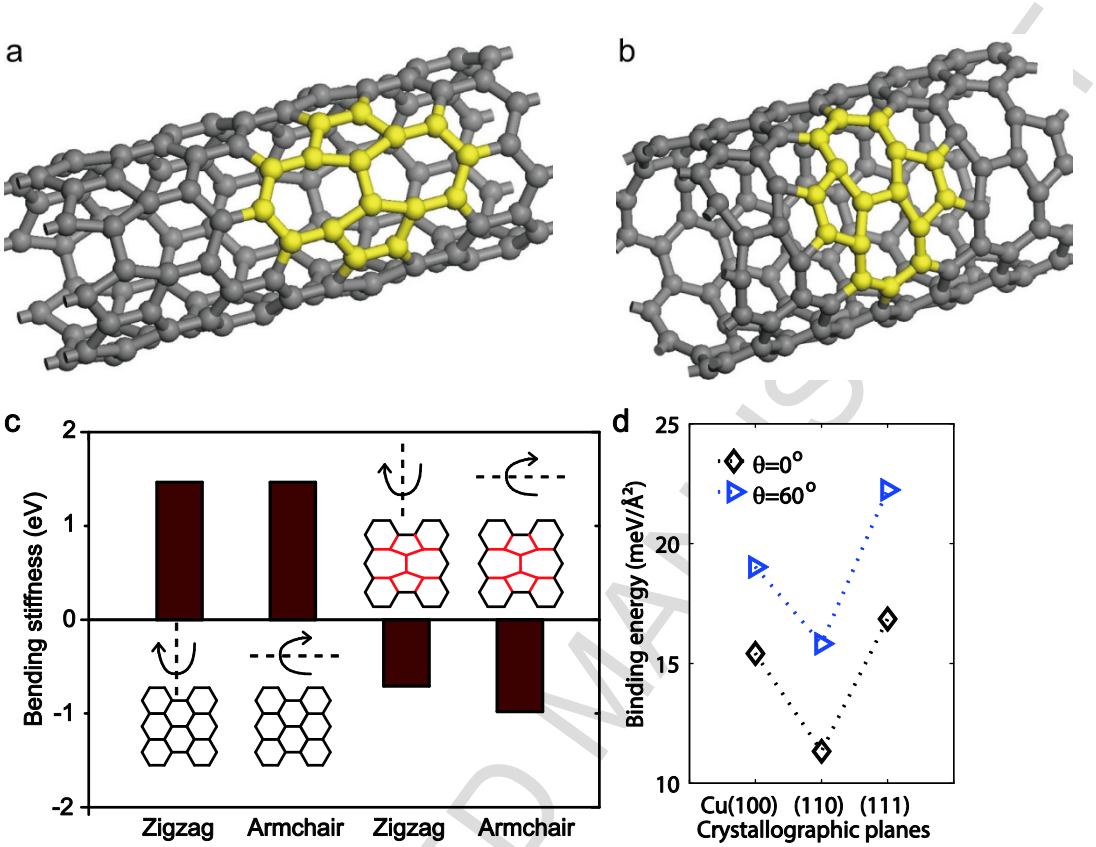

Fig. 5 Atomic structure of graphene with SWA rolling to form nanotube along different chirality: (a) the *x*-axis of a SW being parallel to the tube axis; (b) the *y*-axis of a SW along the tube axis. (c) Bending stiffness of pristine and defective graphene with different chirality. (d) Binding energy of graphene with high density of SWA on different Cu crystallographic planes.

Besides, we calculated the binding energy of graphene with high density of SWA ($\theta = 0°$ and $\theta = 60°$) adhering to different Cu substrates when we cool the system to 300 K. In Fig. 5(d), the value of binding energy is in accordance with that of pristine graphene on copper substrates, Cu (111)> Cu (100) >Cu (110). The binding energy of SWA with $\theta = 60°$ is similar to that of pristine graphene on copper substrate (Cu (100): 19.5 meV/Å, Cu (110): 17.7 meV/Å and Cu (111): 24.1 meV/Å) [12]. However, the binding energy of defective graphene with SWA of θ

= 0° is significantly reduced regardless of the crystallographic planes.

4. Wrinkling in Graphene with Grain Boundaries

Another type of line defects, grain boundaries (GBs), was also commonly observed in large-area CVD graphene samples. We performed the same type of MD simulations to show how the presence of GBs in polycrystalline graphene influences wrinkling. We considered two types of grain boundaries, one with small GB misorientation (5.7°) and the other with very high GB misorientation (27.8°). For details to generate such GBs, the reader is referred to references [45, 46]. In both cases, a major wrinkle parallel to GB direction and a minor wrinkle perpendicular to GB direction are formed, (Figs. 6(a)~(f)). The presence of GBs leads to pristine graphene rotation, and influences the interaction between graphene and the substrates. The wrinkles coincide with the GB when graphene resides on Cu (100) and Cu (111) substrates, but that is not necessary for the Cu (110) substrate.

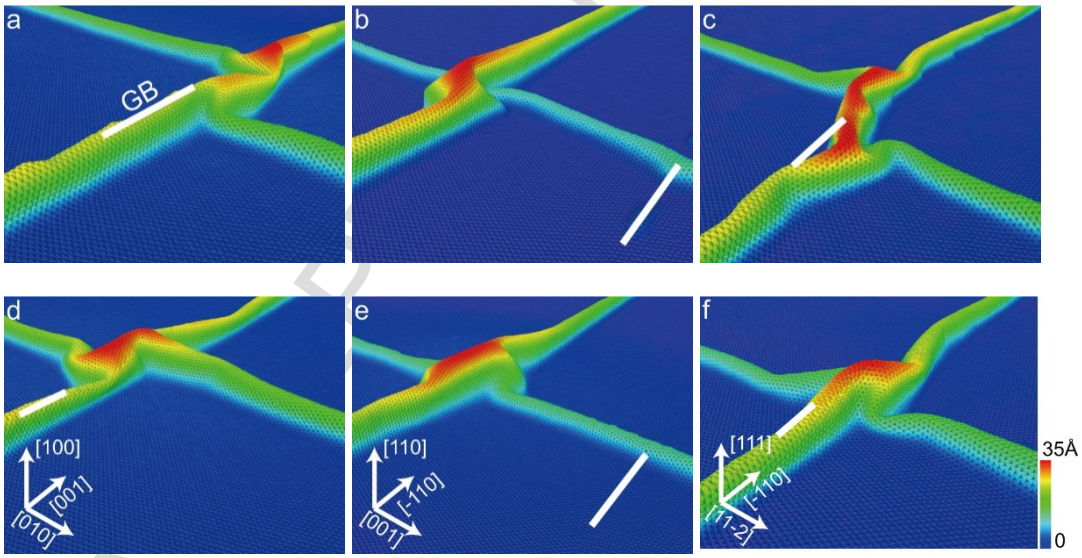

Fig.6 The morphology of polycrystalline graphene films on Cu substrates with different crystallographic planes: (a)~(c) polycrystalline graphene with grain boundary misorientation 5.7° adhering to Cu (100), Cu (110) and Cu (111) respectively; (d)~(f) polycrystalline graphene with grain boundary misorientation 27.8° adhering to Cu (100), Cu (110) and Cu (111) respectively. White lines represent the grain boundary.

In order to distinguish the influence of GBs, we also calculated the binding energy of free graphene with GBs, are shown in Fig. 7(a). Considering the different number of atoms in GBs of different misorientations, we calculated the binding energy per atom. We find the energy of the low angle GB (5.7°) is much lower than the pristine one. It is attributed to the tents formed by the GB defects (Fig. 7(b)). In contrast, the GB region in the sample of high angle GB (27.8°) is nearly flat. The binding energy is similar to that of the pristine one (Fig. 7(c)). Considering bending stiffness of graphene and graphene–substrate adhesion dominate the morphology, we conclude that lower bending stiffness along and perpendicular to the GB, as shown in Fig. 7(a), is the primary factor to guide wrinkle formation.

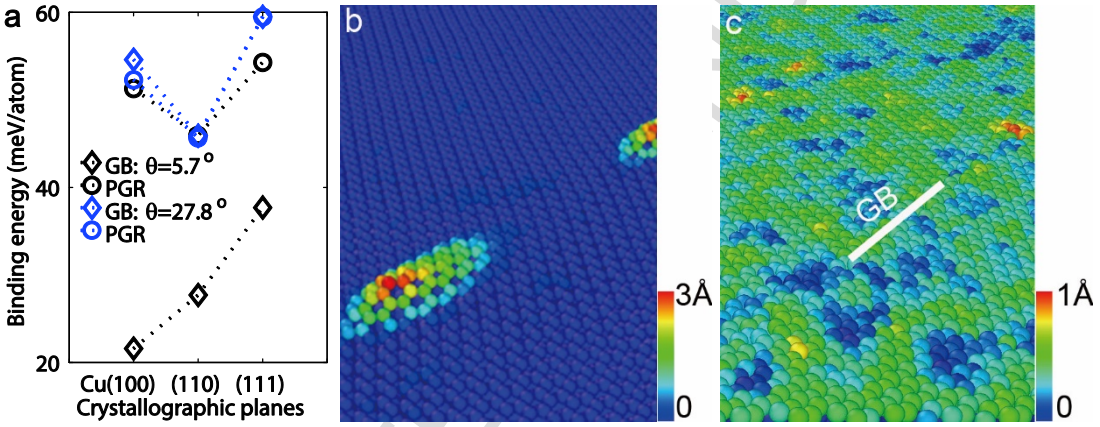

Fig. 7 Wrinkling in graphene with grain boundaries. (a) Binding energy of grain boundary (GB) region and pristine graphene (PGR) region on Cu substrates with different crystallographic planes. The morphology of polycrystalline graphene with different GB misorientation: (b): 5.7° and (c): 27.8°.

5. Experimental verification

To verify our MD simulations, we further experimentally investigated the wrinkling behavior dependent on the linear defects (grain boundary) in graphene. Graphene was grown on Cu(111) single crystal substrate and Cu(100) single crystal substrate by atmospheric pressure chemical vapor deposition (APCVD). The Cu substrates were firstly annealed at 1000 °C with 500 sccm Ar and 10 sccm H_2 at

atmospheric pressure using a tube furnace (Thermal Scientific) for 1 hour. Then, 10 sccm CH_4 (0.1%, diluted in Ar) was introduced for graphene growth. Graphene domain with the size of ~20 μm was obtained after 20-min growth. The full covered graphene film was obtained by extending the growth time to 2 hrs. After growth, CH_4 was switched off and the samples were rapidly cooled down to room temperature. The SEM images of graphene samples were obtained using a Hitachi S4800 field-emission scanning electron microscope (with voltage of 2 kV and current of 10 nA).

Graphene domains was grown on Cu(111) and Cu(100) single crystals using APCVD with very high ratio of H_2/CH_4 ~ 1000. In this scenario, the graphene domains have regular hexagonal shape and all the edges are terminated by zigzag.[47] Hence, the title angle of the grain boundary between two stitched graphene domains can be roughly determined by just measuring the orientation deviation of two stitched graphene domains. As shown in Fig. 8(a), the red and blue line are the zigzag edges of the two graphene domains on Cu(111), and the graphene boundary angle (α) is ~25º. The graphene is ultrasmooth inside the domains, while a wrinkle is visible at the stitching frontier. A smaller grain boundary angle of α ~ 3º also results in a wrinkle at the grain boundary (Fig. 8(b)). In contrast, if the graphene domains are seamless stitched, as in the case of α ~ 0º,[48] there isn't any wrinkle exists at both the inside of domains and the stitching frontier (Fig. 8(c)). The similar phenomena is observed for graphene grown on Cu(100) substrates, that the wrinkle forms at the grain boundary position of two domains (Fig. 8(d)), while no wrinkle exists if the two domains are seamless stitched (Fig. 8(e)). Moreover, we find that graphene wrinkles on Cu(100) substrates are distributed in two vertical directions to form the cross structure, which resembles the stimulation results (Fig. 8(f)).

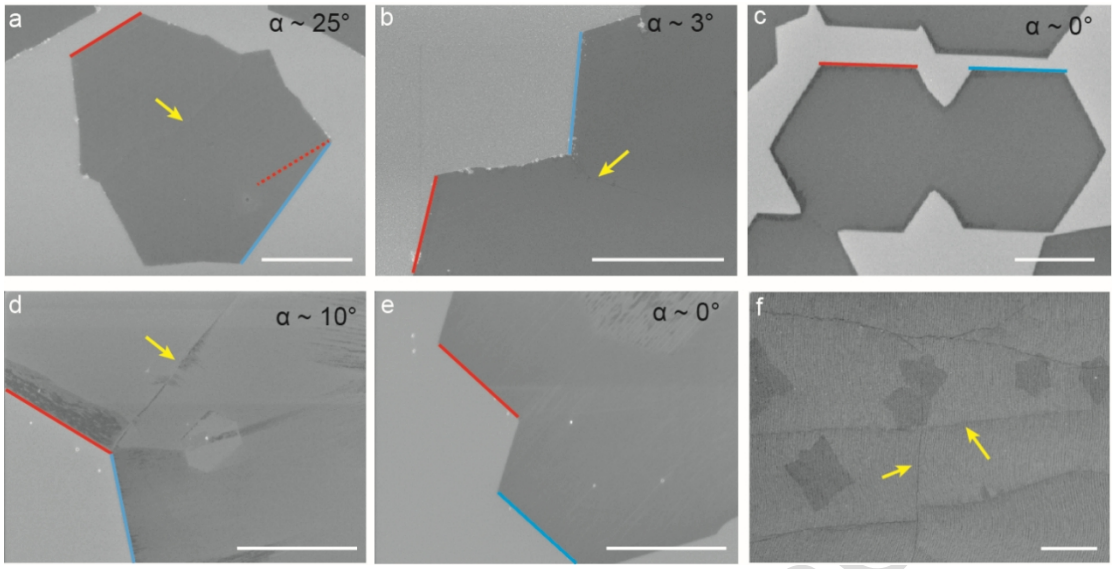

Fig.8 Wrinkles formation of graphene grown on Cu substrates. (a-c) SEM images of graphene domains grown on Cu(111) substrates. (d-f) SEM images of graphene grown on Cu(100) substrates. The zigzag edges of left and right domains are labeled in red line and blue line, respectively. The wrinkles are indicated by yellow arrows. α represents the title grain boundary angle. Scale bars: 10 μm (a, b, c, f), 5 μm (d, e).

As shown in Figure 9a, a graphene wrinkle was visualized using AFM morphology imaging by contact mode. The height profile of the wrinkles is shown in Figure 9b. Because the Cu substrate is rough, we deduct the baseline of the Cu substrate and got the height value of this wrinkle being ~ 2 nm. Furthermore, more than 40 graphene wrinkles were scanned to obtain the height distribution shown in Figure 9c. The height of the graphene wrinkles range could be as high as 7 nm, with a mean about 2 nm.

To extract information on the defectivity of graphene in wrinkled region, graphene grown on Cu foil was transferred onto SiO2/Si substrates, as shown in Figure 9c. The Raman spectra of the planar graphene and wrinkled graphene was shown in Figure 9e. Compared to the planar region, the wrinkled region has obvious D band, indicating that there are defects in the wrinkle region. However, it is worth noting here that the defect band cannot be simply ascribed to structural defects, since the curving of graphene lattice also enables the radial breathing mode [49].

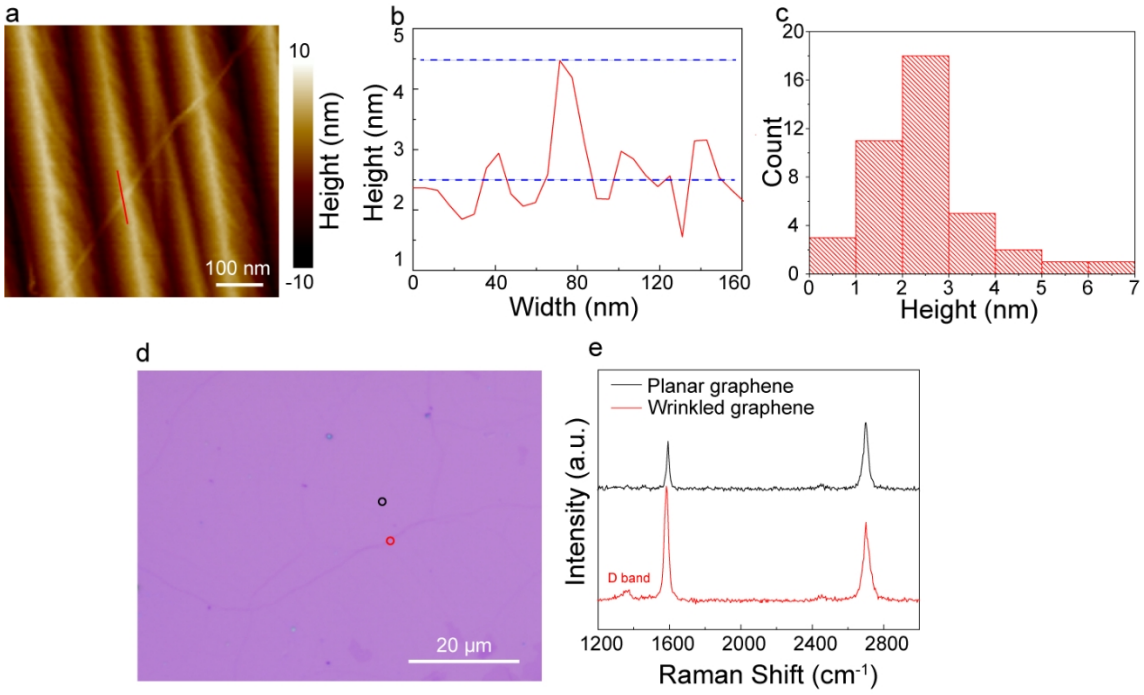

Figure 9. Characterization of graphene wrinkles by AFM and Raman. (a) AFM morphology image of graphene wrinkles on Cu substrates. (b) Height profile of a graphene wrinkle. (c) Height distribution of graphene wrinkles on Cu substrates. (d) OM image of graphene transferred onto SiO_2/Si substrate. (e) Raman spectrum of wrinkled graphene and planar graphene.

6. Discussion and Conclusion

To further our understanding regarding wrinkling in graphene on different crystallographic planes of copper substrate, we show in this work how typical defects like Stone-wales arrays and grain boundaries influence the morphology of graphene prepared by CVD method. For SWAs, it is revealed the orientation of the arrays w.r.t. graphene, the density of the SW defects, the orientation of the graphene w.r.t. the substrate, and the crystallographic planes of a Cu substrate all affect the pattern of wrinkles. Those factors may influence either the bending stiffness of graphene or the binding energy of graphene-Cu substrate, and these two parameters govern the morphology of graphene sheets on a substrate. Even though the Cu (1 0 0) and Cu (1 1 0) have the lower binding energy, the competition of these factors can eliminate the wrinkling when graphene grown on Cu (1 0 0) and Cu (1 1 0) when the orientation of

SW is perpendicular to the direction of SWA ($\theta = 0°$, $\phi = 90°$). The orientation of SW plays a dominant role in determining the direction of wrinkles. In the presence of grain boundaries, we see the formation of two cross wrinkles, with the primary one being parallel to the GB direction and the second one roughly perpendicular to the GB. We attribute these morphology changes to the weakening of bending stiffness in graphene nearby the GB region and also relative orientation between the graphene and the substrate. The latter affects the binding energy of graphene-Cu substrate. At the end, we present experimental observations on wrinkling in polycrystalline graphene. Our simulations and analysis match qualitatively well with the experimental results. The research on wrinkling in defective graphene helps us understand the origin of wrinkling in CVD graphene and also help to efficient graphene transfer using mechanical methods [50].

Acknowledgments

YW acknowledges the support from National Natural Science Foundation of China (NSFC) (11425211). The calculations are performed at the Supercomputing Center of CAS.

References

1. Li, X., et al., *Large-area synthesis of high-quality and uniform graphene films on copper foils.* Science, 2009. **324**(5932): p. 1312-1314.
2. Chae, S.J., et al., *Synthesis of large ‐area graphene layers on poly ‐nickel substrate by chemical vapor deposition: wrinkle formation.* Advanced Materials, 2009. **21**(22): p. 2328-2333.
3. Gao, L., et al., *Repeated growth and bubbling transfer of graphene with millimetre-size single-crystal grains using platinum.* Nature communications, 2012. **3**: p. 699.
4. Seeley FB, S.J., *Advanced mechanics of materials.* Wiley, New York, 1952: p. 342.
5. Yoon, D., Y.-W. Son, and H. Cheong, *Negative thermal expansion coefficient of graphene measured by Raman spectroscopy.* Nano letters, 2011. **11**(8): p. 3227-3231.
6. Chen, S., et al., *Thermal conductivity measurements of suspended graphene with and without wrinkles by micro-Raman mapping.* Nanotechnology, 2012. **23**(36): p. 365701.
7. Vasić, B., A. Zurutuza, and R. Gajić, *Spatial variation of wear and electrical properties across wrinkles in chemical vapour deposition graphene.* Carbon, 2016. **102**: p. 304-310.
8. Lópezpolín, G., et al., *Increasing the elastic modulus of graphene by controlled defect creation.* Nature Physics, 2015. **11**(1): p. 26-31.
9. Giannazzo, F., et al., *Fabrication and Characterization of Graphene Heterostructures with Nitride Semiconductors for High Frequency Vertical Transistors.* Phys. Status Solidi A, 2018. **215**(10): p. 1700653.
10. Muneer, A., et al., *Nanoscale investigation of charge transport at the grain boundaries and wrinkles in graphene film.* Nanotechnology, 2012. **23**(28): p. 285705.
11. Lahiri, J., et al., *An extended defect in graphene as a metallic wire.* Nat Nano, 2010. **5**(5): p. 326-329.
12. Deng, B., et al., *Wrinkle-Free Single-Crystal Graphene Wafer Grown on Strain-Engineered Substrates.* ACS Nano, 2017. **11**(12): p. 12337-12345.
13. Wood, J.D., et al., *Effects of Polycrystalline Cu Substrate on Graphene Growth by Chemical Vapor Deposition.* Nano Letters, 2011. **11**(11): p. 4547-4554.
14. Gao, L., J.R. Guest, and N.P. Guisinger, *Epitaxial Graphene on Cu(111).* Nano Letters, 2010. **10**(9): p. 3512-3516.
15. Zhao, L., et al., *Influence of copper crystal surface on the CVD growth of large area monolayer graphene.* Solid State Communications, 2011. **151**(7): p. 509-513.
16. Park, S. and R.S. Ruoff, *Chemical methods for the production of graphenes.* Nature nanotechnology, 2009. **4**(4): p. 217-224.
17. Hashimoto, A., et al., *Direct evidence for atomic defects in graphene layers.* Nature, 2004. **430**(7002): p. 870.
18. Yu, Q., et al., *Control and characterization of individual grains and grain boundaries in graphene grown by chemical vapour deposition.* Nature Materials, 2011. **10**: p. 443.
19. Pan, M., et al., *Topographic and Spectroscopic Characterization of Electronic Edge States in CVD Grown Graphene Nanoribbons.* Nano Letters, 2012. **12**(4): p. 1928-1933.
20. Wei, Y. and R. Yang, *Nanomechanics of graphene.* National Science Review, 2018: p. https://doi.org/10.1093/nsr/nwy067.
21. Tapasztó, L., et al., *Breakdown of continuum mechanics for nanometre-wavelength rippling of*

graphene. Nature Physics, 2012. **8**: p. 739.

22. Kim, S.J., et al., *Ultraclean Patterned Transfer of Single-Layer Graphene by Recyclable Pressure Sensitive Adhesive Films.* Nano Letters, 2015. **15**(5): p. 3236-3240.
23. Hattab, H., et al., *Interplay of Wrinkles, Strain, and Lattice Parameter in Graphene on Iridium.* Nano Letters, 2012. **12**(2): p. 678-682.
24. Zhang, T., X. Li, and H. Gao, *Designing graphene structures with controlled distributions of topological defects: A case study of toughness enhancement in graphene ruga.* Extreme Mechanics Letters, 2014. **1**: p. 3-8.
25. Zhang, T., X. Li, and H. Gao, *Defects controlled wrinkling and topological design in graphene.* Journal of the Mechanics and Physics of Solids, 2014. **67**: p. 2-13.
26. Li, J., *Disclination model of high angle grain boundaries.* Surface Science, 1972. **31**: p. 12-26.
27. White, G., *Thermal expansion of reference materials: copper, silica and silicon.* Journal of Physics D: Applied Physics, 1973. **6**(17): p. 2070.
28. Plimpton, S., *Fast parallel algorithms for short-range molecular dynamics.* Journal of computational physics, 1995. **117**(1): p. 1-19.
29. Stuart, S.J., A.B. Tutein, and J.A. Harrison, *A reactive potential for hydrocarbons with intermolecular interactions.* The Journal of chemical physics, 2000. **112**(14): p. 6472-6486.
30. Foiles, S., M. Baskes, and M. Daw, *Embedded-atom-method functions for the fcc metals Cu, Ag, Au, Ni, Pd, Pt, and their alloys.* Physical review B, 1986. **33**(12): p. 7983.
31. Shi, X., Q. Yin, and Y. Wei, *A theoretical analysis of the surface dependent binding, peeling and folding of graphene on single crystal copper.* Carbon, 2012. **50**(8): p. 3055-3063.
32. Chen, H. and S. Chen, *The peeling behaviour of a graphene sheet on a nano-scale corrugated surface.* Journal of Physics D: Applied Physics, 2013. **46**(43): p. 435305.
33. Yufeng, G. and G. Wanlin, *Structural transformation of partially confined copper nanowires inside defected carbon nanotubes.* Nanotechnology, 2006. **17**(18): p. 4726.
34. Kresse, G. and J. Furthmüller, *Efficiency of ab-initio total energy calculations for metals and semiconductors using a plane-wave basis set.* Computational Materials Science, 1996. **6**(1): p. 15-50.
35. Kresse, G. and J. Furthmüller, *Efficient iterative schemes for ab initio total-energy calculations using a plane-wave basis set.* Physical Review B, 1996. **54**(16): p. 11169-11186.
36. Blöchl, P.E., *Projector augmented-wave method.* Physical Review B, 1994. **50**(24): p. 17953-17979.
37. Kresse, G. and D. Joubert, *From ultrasoft pseudopotentials to the projector augmented-wave method.* Physical Review B, 1999. **59**(3): p. 1758-1775.
38. Perdew, J.P., K. Burke, and M. Ernzerhof, *Generalized Gradient Approximation Made Simple.* Physical Review Letters, 1996. **77**(18): p. 3865-3868.
39. Perdew, J.P., K. Burke, and M. Ernzerhof, *Generalized Gradient Approximation Made Simple [Phys. Rev. Lett. 77, 3865 (1996)].* Physical Review Letters, 1997. **78**(7): p. 1396-1396.
40. Wei, Y., et al., *Bending rigidity and Gaussian bending stiffness of single-layered graphene.* Nano letters, 2012. **13**(1): p. 26-30.
41. Wilder, J.W.G., et al., *Electronic structure of atomically resolved carbon nanotubes.* Nature, 1998. **391**: p. 59.
42. Yin, H., et al., *Griffith Criterion for Brittle Fracture in Graphene.* Nano Letters, 2015. **15**(3): p. 1918-1924.

43. Monkhorst, H.J. and J.D. Pack, *Special points for Brillouin-zone integrations.* Physical Review B, 1976. **13**(12): p. 5188-5192.
44. Kudin, K.N., G.E. Scuseria, and B.I. Yakobson, *C2F, BN, and C nanoshell elasticity from ab initio computations.* Physical Review B, 2001. **64**(23): p. 235406.
45. Wu, J. and Y. Wei, *Grain misorientation and grain-boundary rotation dependent mechanical properties in polycrystalline graphene.* Journal of the Mechanics and Physics of Solids, 2013. **61**(6): p. 1421-1432.
46. Wei, Y., et al., *The nature of strength enhancement and weakening by pentagon–heptagon defects in graphene.* Nature materials, 2012. **11**(9): p. 759-763.
47. Ma, T., et al., *Edge-controlled growth and kinetics of single-crystal graphene domains by chemical vapor deposition.* Proc Natl Acad Sci U S A, 2013. **110**(51): p. 20386-91.
48. Nguyen, V.L., et al., *Seamless Stitching of Graphene Domains on Polished Copper (111) Foil.* Advanced Materials, 2015. **27**(8): p. 1376-+.
49. Gupta, A.K., et al., *Curvature-induced D-band Raman scattering in folded graphene.* Journal of Physics: Condensed Matter, 2010. **22**(33): p. 334205.
50. Fisichella, G., et al., *Microscopic mechanisms of graphene electrolytic delamination from metal substrates.* Applied Physics Letters, 2014. **104**(23): p. 233105.

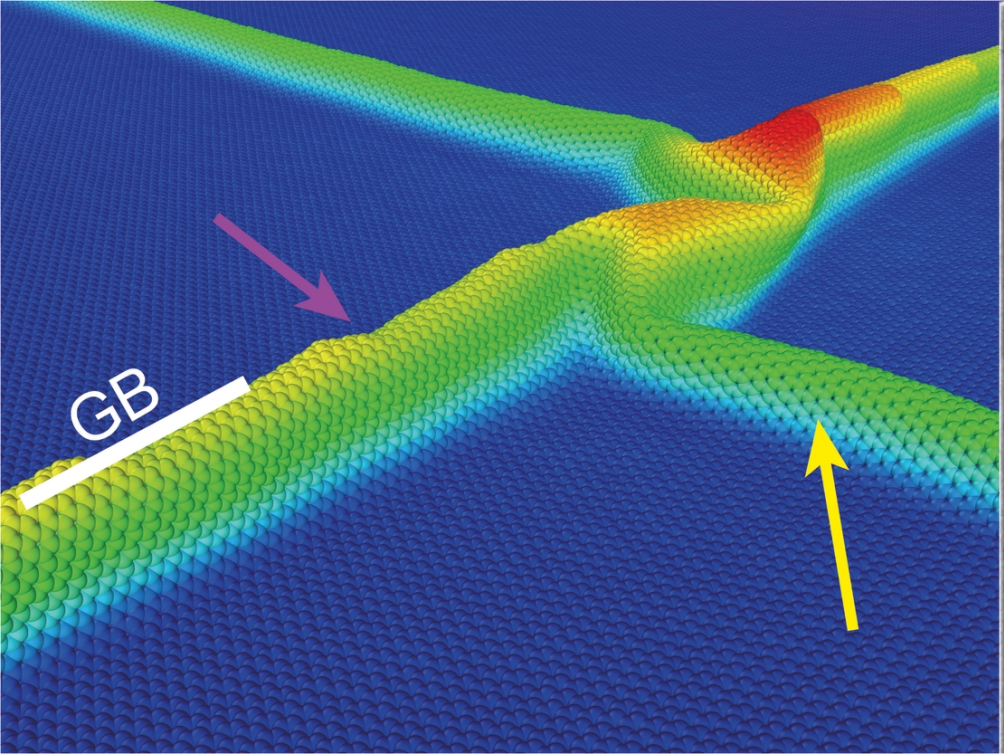
GB

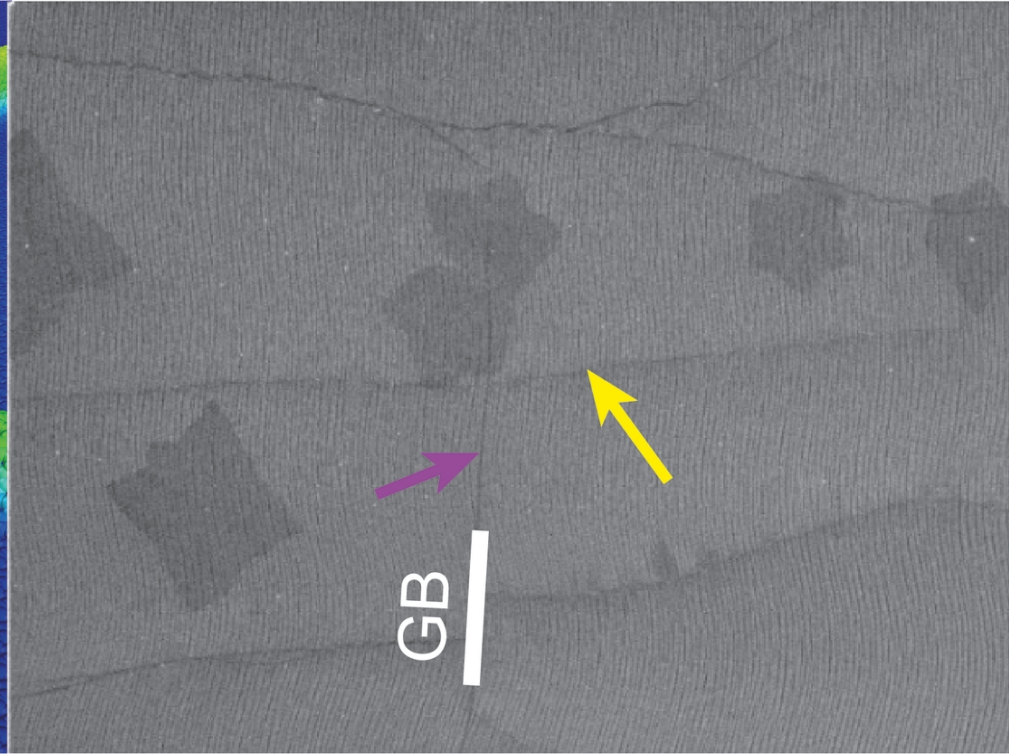
GB